"BABEŞ-BOLYAI" UNIVERSITY, CLUJ-NAPOCA
FACULTY OF MATHEMATICS AND COMPUTER SCIENCE

THE ORIGIN AND EVOLUTION OF CELESTIAL BODIES GRAVITATING IN THE VICINITY OF EARTH'S ORBIT

-doctoral thesis-
EXTENDED ABSTRACT

Ştefan Gh. Berinde

Research supervisor: Prof. Dr. Vasile Ureche

June 2002

Additional information about this work can be found at the following internet address:
http://math.ubbcluj.ro/∼sberinde/thesis

Thesis content

Introduction

The solar system is a fascinating place in the Universe. One century ago, it was thought that this place is dominated by order, where several well defined classes of celestial bodies are hierarchically disposed in space. But this image has radically changed in our days. Many observational data, enriched by theoretical results, reveal the "new" solar system as a tumultuous region, where millions of interplanetary bodies of different sizes follow their own orbital destinies, in a chaotic manner, where gravitational captures and collisional processes are current realities.

Nowadays, the advanced observational technique transforms the mysterious dots of light from the sky in well individualized bodies, with their own physical and dynamical characteristics, history and origin. Some of them have peculiar orbits, allowing a close encounter with the Earth, sometimes at distances very uncomfortable for us, the earthlings.

The geological evolution of our planet and even of life in the past eras, it seems that have been influenced by the presence of such a population of bodies in the vicinity of Earth's orbit. The impact danger haven't passed, but besides of the effort undertaken by the humanity to detect the most threatening ones, these bodies are also viewed as easy-to-reach targets for the next space missions. And this dream became already a reality, since the NEAR space vehicle has landed on the surface of asteroid Eros - one of the most representative members of this population.

The topic about origin and evolution of celestial bodies gravitating in the vicinity of Earth's orbit is a wide multidisciplinary field of research. This work synthesizes the most important results obtained in the last years and expands those sections where the author brought his contribution.

Chapter 1 makes a short description of this population and gives some orbital classifications based one the accumulated observational material. The effect of observational biases is highlighted and some estimates about the real pattern of this population are given.

Close encounters with the inner planets are a distinctive dynamical characteristic of these bodies, and chapter 2 is fully dedicated to this phenomenon. Two classical approaches are considered: one is given in the frame of restricted three-body problem and the other one is based on Öpik's geometric formalism. Here, some classical results are analyzed and an extension of this theory is proposed by the author [Berinde, 2001a]. Section 2.2.4 deals with this extension, where a complete map of orbital changes due to a close encounter is formulated. This map consists in obtaining analytical expressions connecting the six pre-encounter and post-encounter orbital elements of the body, based on the well known simplificative assumptions of Öpik. The map is later used (on section 4.2.2) as the dynamical engine of a proposed diffusion process of trans-neptunian bodies throughout the outer solar system, which is solely based on the scattering effect of multiple close encounters with the giant planets.

Dynamical evolution of celestial bodies in the vicinity of Earth is studied in chapter 3. First of all, we underline here the chaotic behaviour of their motion, with major implications on the deterministic aspect of long-term numerical simulations. In several situations, these simulations are the only gate that we have to look for some dynamical characteris-

tics of a motion. Next, we describe the resonant motions and their associated protection mechanisms against close encounters. After an extensive numerical study, we identify three types of dynamical evolutions of these orbits in the vicinity of Earth, based on the long-term dynamical behaviour of the minimal orbital intersection distance: short-time orbital approach, periodic orbital approach and long-time orbital approach [Berinde, 1999b]. This study is similar in some aspects to that of [Carusi and Dotto, 1996].

The problem of identifying the source regions of the bodies from the vicinity of Earth and their associated transport mechanisms, represents a major challenge for modern celestial mechanics, and chapter 4 synthesizes the main results and hypothesis in this regard. It is mainly described the role of inter-asteroidal collisions coupled with the resonance processes in the main belt. In the second part of the chapter, we describe the cometary component of our population of bodies. We propose at this point the model of chaotic diffusion discussed above. Based on it, we give several statistical results about the origin of short-period comets in the Kuiper belt [Berinde, 2001a]. These estimates include: the frequency of close encounters with the giant planets mapped onto phase space of orbital elements, the percent of dynamical end-states and various dynamical lifetimes. We evaluate about 42% of the bodies which are already driven into Neptune-crossing orbits will enter in the cometary active region as short-period comets, at some time during their dynamical history in the solar system.

A major impulse given to the research in this field is the threatening nature of an impact with the Earth, that may occur in the future. Chapter 5 is an incursion in the topic of estimating the impact probability with the Earth, presenting three well known methods of computation, accompanied by some examples of their applicability on real bodies. The first two methods give mean values of the probability on a certain interval of time, firstly, by extrapolating the frequency of close encounters, and secondly, by averaging the collision probability along the bodies' orbit. Third method, which is far more complex, is naturally obtained from the theory of orbit determination and is based on the propagation of initial orbital uncertainty region of the body. The propagation of this uncertainty region, in the frame of circular, restricted three-body problem, is another contribution of the author at this work (section 5.2.2). Using the Öpik's geometric formalism, we are able to compute through analytic formulas the dispersion of the orbital uncertainty during a close encounter with the planet. We identify also an oscillatory behaviour of the uncertainty along the orbit [Berinde, 2001b], which seems to be characteristically to many asteroidal orbits in the vicinity of Earth.

Many aspects from our study performed in chapter 5 are related to the Monte-Carlo sampling technique. Another contribution of the author is the section 5.2.6, where we propose an iterative sampling method for the initial uncertainty region, in order to identify the set of virtual impactors of a given close encounter and to compute the intrinsic probability of the impact [Berinde, 2002]. Our method is based on a topologic analysis performed in the six-dimensional space of orbital elements, with the purpose of isolating, as closely as possible, the entire set of virtual impactors. By estimating the probability density of the orbital elements in the last sampled region, we obtain the associated impact probability. The total number of used sampling points is several orders of magnitude lower than the inverse of the impact probability to be computed, and this gives a practical applicability to our method. In this manner, we have computed the impact probabilities

for the asteroids 2000 SG_{344} and 2001 BA_{16}. At the end of the chapter we describe the Torino and Palermo scales, used for quantifying the impact hazard and, finally, some estimates about the impact consequences on Earth are given.

Many parts of this work are based on extensive numerical simulations. Because of this reason, we present in chapter 6 a package of programs for manipulating dynamical systems of bodies, especially created to help us in this research. The SolSyIn package is based on the well known Radau-Everhart numerical integrator, which is optimized for accurately handling close encounters. Many other numerical algorithms are added to this, in order to compute various dynamical parameters described in the previous chapters and to generate the plots of dynamical evolutions. This software is available on internet at the address given in the reference [Berinde, 2001c].

*

I would like to express gratitude to my supervisor, professor dr. Vasile Ureche, for his accurate guidance during my graduate study at Babes-Bolyai University and for his valuable suggestions that considerably improved the final version of this work. I am also pleased to acknowledge the support came from the staff of Mechanics and Astronomy Department of our Faculty and from the staff of researchers of the Astronomical Institute of Romanian Academy in Cluj-Napoca.

Abbreviations

ECA - Earth-crossing asteroid
LCE - Lyapounov characteristic exponent
LOV - line of variation (of the uncertainty region)
NEA - near-Earth asteroid
MOID - minimal orbital intersection distance
PHA - potentially hazardous asteroid
UA - astronomical unit of distance (mean distance Earth-Sun)

Chapter 1. Population description

1.1 Observational evidences

First of all, we define de concept of vicinity of Earth's orbit (commonly termed as near-Earth space), i.e. the region in the phase space of orbital elements given by the inequalities $q < 1.3$ UA and $Q > 0.983$ UA, where q and Q denotes the distances to perihelion and aphelion of the body's orbit. Dynamically speaking, the members of this population include: asteroids, comets and meteoroids, but the later ones do not make the subject of the paper. These asteroids, called near-Earth asteroids (NEA), represent the majority of the population, since the number of active comets in this region is quite small and the extinct cometary nuclei are catalogued as cometary asteroids, so they are also NEA.

The increased discovery rate of NEAs in the last years is underlined (figure 1).

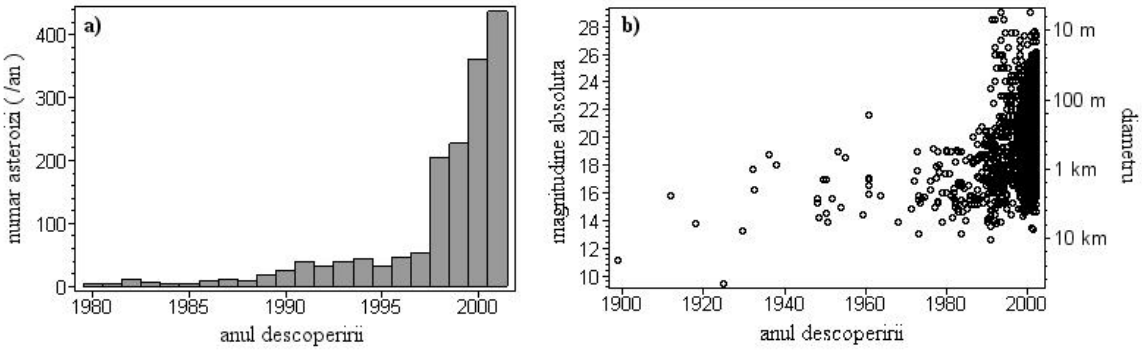

Figure 1: a) annual discovery rate of NEAs and b) discovery distribution in time against the body's absolute magnitude (or its diameter).

Afterwards, we define the Atens, Apollos and Amors classes and also the Earth-crossing asteroids class (ECA) [Dvorak, 1999].

1.2 Observational biases

NEAs are discovered preponderantly when they pass near Earth, and those with higher albedos are more easily seen. Generally, the observing window is narrow, so we have to wait for the next close encounter in order to improve the orbit and to decrease the orbital uncertainty. These are observational biases and they affect the observed distribution of this population in the phase space of orbital elements. Trying to correct this, we can give estimates about the real population [Rabinowitz *et al.*, 1994], [Bottke *et al.*, 2000].

Figure 2 shows the amount of discovery completeness at various sizes and an estimation of the real number of NEAs. Finally, the mean collisional time with the Earth is derived, which is based on previous estimates about the unbiased population.

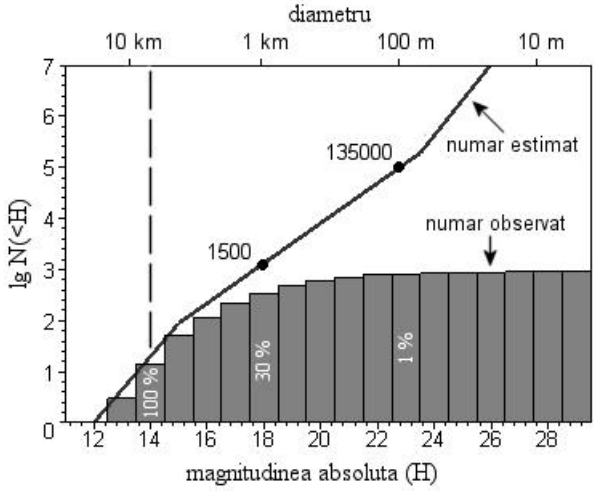

Figure 2: Cumulative number of discovered NEAs till 1st of January 2002 and the estimated number of the entire population, function of the body's absolute magnitude (or its diameter).

Chapter 2. Dynamics of close encounters

When the asteroid (thought as an infinitesimal body) moves inside the gravitational sphere of action of a planet, we consider that it makes a close encounter with that planet.

2.1 The restricted three-body problem

Starting with the equations of motion for the circular case, written in two reference frames, namely: the inertial one, with the origin in the primary, having unity mass, and the corotational one (moving synchronously with the secondary body of mass m_p - the perturbatrice planet), with the origin in the baricenter of the system, we deduce several expressions for the Jacobi integral, as follows [Tisserand, 1896], [Murray and Dermott, 1999]:

-in the inertial frame

$$\left(\frac{\mathrm{d}\mathbf{r}}{\mathrm{d}t}\right)^2 - 2G\left[\frac{1}{r} + m_p\left(\frac{1}{d} - \frac{\mathbf{r}\mathbf{r}_p}{a_p^3}\right)\right] - 2\mathbf{n}\cdot\left(\mathbf{r}\times\frac{\mathrm{d}\mathbf{r}}{\mathrm{d}t}\right) = -C_J\,(\text{constant}), \tag{1}$$

where $\mathbf{r}, \mathbf{r}_p$ are the position vectors of the infinitesimal body and, respectively, of the planet and d is the distance between them; a_p, n_p are the radius of the planet's orbit and its daily mean motion, $\mathbf{n} = (0, 0, n_p)$ and G is the heliocentric gravitational constant;

-in the corotational frame

$$\dot{\xi}^2 + \dot{\eta}^2 + \dot{\zeta}^2 = 2U - C_J, \tag{2}$$

where (ξ, η, ζ) denote the coordinates of the infinitesimal body and

$$U = G\,\frac{1}{r} + Gm_p\,\frac{1}{d} + \frac{n_p^2}{2}(\xi^2 + \eta^2) \tag{3}$$

is the total potential;

- function of the keplerian orbital elements (a, e, I)

$$\frac{1}{a} + 2\frac{\sqrt{1+m_p}}{a_p}\sqrt{\frac{a}{a_p}(1-e^2)} \cdot \cos I + m_p\left(\frac{2}{d} + \frac{d^2 - r^2 - a_p^2}{a_p^3}\right) = G^{-1}C_J. \tag{4}$$

Neglecting the mass of the planet ($m_p \ll 1$), we have the Tisserand criterion

$$\frac{a_p}{a} + 2\sqrt{\frac{a}{a_p}(1-e^2)} \cdot \cos I = T\,(\text{constant}). \tag{5}$$

Writing the potential U in a suitable form, for the planar case, and imposing the conditions for equilibrium, we derive the locations of the five Lagrange equilibrium points in the bidimensional space of motion and also on the corresponding zero-velocity surface ($C_J = 2U$). At a later time, we will identify types of orbits related to these points.

Approximating the equations of motion near the perturbatrice body in a suitable form, we obtain the Hill's equations

$$\begin{cases} \ddot{\xi} - 2n_p\dot{\eta} = G\left(\dfrac{3}{a_p^3} - \dfrac{m_p}{d^3}\right)\xi = \dfrac{\partial U_H}{\partial \xi} \\ \\ \ddot{\eta} + 2n_p\dot{\xi} = -Gm_p\dfrac{\eta}{d^3} = \dfrac{\partial U_H}{\partial \eta} \end{cases} \tag{6}$$

and a new expression for the potential

$$U_H = G\left(\frac{3\xi^2}{2a_p^3} + \frac{m_p}{d}\right), \quad d^2 = \xi^2 + \eta^2. \tag{7}$$

When the acceleration along the ξ axis vanishes (that is, on the direction to the primary), we obtain the expression for the radius of Hill's (gravitational) sphere of action

$$s_p = a_p\left(\frac{m_p}{3}\right)^{\frac{1}{3}}. \tag{8}$$

2.2 Öpik's geometric formalism

We consider here the Öpik's approach of the three-body problem as two two-body problems, depending on the position of the infinitesimal body in respect to the sphere of action of the planet [Öpik, 1963], [Carusi *et al.*, 1990].

When we refer to the motion of the body outside the planetary sphere of action, its planetocentric unperturbed velocity near the planet, $\mathbf{u} = \mathbf{v} - \mathbf{v}_p$, is a key quantity, since its magnitude is an invariant during the close encounter. From geometric considerations and in the frame of some simplificative assumptions, which will be described below, we can derive its expression as follows

$$u^2 = v_p^2\left[3 - \left(\frac{a_p}{a} + 2\sqrt{\frac{a}{a_p}(1-e^2)} \cdot \cos I\right)\right], \tag{9}$$

and also in function of the Tisserand parameter, $u = v_p\sqrt{3-T}$, where v_p denotes the circular velocity of the planet on its orbit. The condition $0 < T < 3$ is shown that characterizes the crossing orbits in respect to that of the planet.

Through a parametrization of the velocity vector $\mathbf{u}$, we obtain the relations between its orientation in space and the corresponding heliocentric orbital elements of the body

$$\begin{cases} a = \dfrac{G}{v_p^2 - 2v_p u\cos\theta - u^2} \\ e = \dfrac{u^2}{v_p^2}\sqrt{1-\sin^2\theta\sin^2\phi + 2\dfrac{v_p}{u}(2-\sin^2\theta\sin^2\phi)\cos\theta + \dfrac{v_p^2}{u^2}(4\cos^2\theta+\sin^2\theta\sin^2\phi)} \\ I = \arctan\left(\dfrac{\sin\theta\cos\phi}{\cos\theta + \dfrac{v_p}{u}}\right), \end{cases} \tag{10}$$

where (θ, ϕ) are the orientation angles. Their inverse expressions are

$$\cos\theta = \frac{v_p^2 - u^2 - G\left(\dfrac{1}{a}\right)}{2v_p u}, \tag{11}$$

$$\cos\phi = \pm\frac{\cos\theta + \dfrac{v_p}{u}}{\sin\theta}\tan I. \tag{12}$$

We have the following chain of relations between the pre-encounter and post-encounter orbital elements of the body (the later ones being denoted with "prime")

$$(a, e, I) \rightarrow (u, \theta, \phi) \rightarrow (u, \theta', \phi') \rightarrow (a', e', I'). \tag{13}$$

The middle implication can be solved by considering the motion inside the planetary sphere of action, where the trajectory of the body is considered to be a hyperbolic planetocentric one. Then we get

$$\cos\theta' = \cos\theta\cos\gamma + \sin\theta\sin\gamma\cos\psi \tag{14}$$

and

$$\cos\mathrm{d}\phi = \frac{\cos\gamma - \cos\theta\cos\theta'}{\sin\theta\sin\theta'}, \quad \sin\mathrm{d}\phi = \pm\frac{\sin\gamma\sin\psi}{\sin\theta'}, \tag{15}$$

where $\mathrm{d}\phi = \phi' - \phi$. In order to solve the problem completely, we have to know the angles (γ, ψ).

The such called gravitational deflection angle γ is given by

$$\tan\frac{\gamma}{2} = \frac{Gm_p}{bu^2} = \frac{R_p}{2b}\left(\frac{v_{par}}{u}\right)^2, \tag{16}$$

where b is the encounter parameter (the planetocentric distance to the asymptotes of the hyperbolic orbit), R_p is the radius of the planetary globe and v_{par} is the parabolic velocity on its surface.

The angle ψ measures the inclination of the plane of planetocentric motion and we will derive an expression for it as a part of the complete map of orbital changes, described below.

We define also on the paper the impact radius r_{imp} and the maximum deflection angle γ_{max} and we give some examples of their variation for various initial conditions.

Our contribution at this point consists in obtaining explicit analytical relations between the pre-encounter and post-encounter heliocentric orbital elements of the body (in standard notations) [Berinde, 2001a]

$$(a, e, I, \Omega, \omega, M) \rightarrow (a', e', I', \Omega', \omega', M'). \tag{17}$$

To accomplish this, we make use of the Öpik's simplificative assumptions:

(i) the motion of the body knows two regimes, the heliocentric and the planetocentric one, depending on its position in respect to the planetary sphere of action;

(ii) the planet is moving on a circular orbit around the Sun;

(iii) the encounter takes place near one of the orbital nodes of the infinitesimal body;

(iv) during the close encounter the unperturbed trajectories of the encountering bodies are supposed to be rectilinear and their unperturbed velocities are constant;

(v) finally, the close encounter acts as an instantaneous impulse and displacement given to the object when it riches the minimum planetocentric distance, in such a way that it is moved from one asymptote of its hyperbolic orbit to the other one.

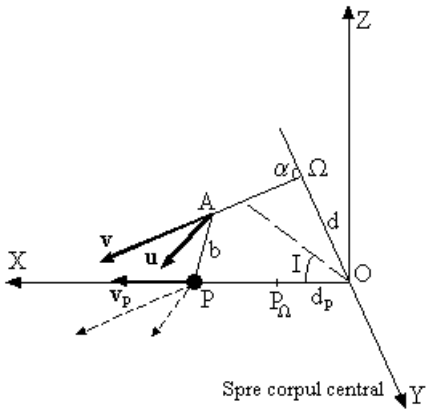

Figure 3: Encounter geometry in the vicinity of line of nodes.

We consider the encounter geometry as in figure 3, where the distances d_p and d play an important role. The first one is the distance between the planet's orbit to the node of the body's orbit and the second one is the distance between the line of nodes to the planet's position, P, at the time t_Ω, when the asteroid passes through its node, i.e.

$$d = a_p - a\frac{1-e^2}{1+\epsilon_{nod}\cos\omega}, \quad d_p = a_p(l_p(t_\Omega) - \Omega), \tag{18}$$

where ϵ_{nod} selects the type of node and $l_p(t)$ is the mean longitude of the planet, a function of time.

The encounter parameter can be expressed as

$$b = \sqrt{b_{moid}^2 + (d\sin\phi\cos\theta + d_p\sin\theta)^2}, \tag{19}$$

where $b_{moid} = |d\cos\phi|$ is the such called minimal orbital intersection distance (MOID).

The expression of the inclination of planetocentric orbit is given by

$$\cos\psi = \frac{(\mathbf{b}\times\mathbf{u})\cdot(\mathbf{u}\times\mathbf{v}_p)}{|\mathbf{b}\times\mathbf{u}|\cdot|\mathbf{u}\times\mathbf{v}_p|}, \tag{20}$$

or alternatively

$$\sin\psi = \frac{b_{moid}}{b}, \tag{21}$$

where the components of the planetocentric angular momentum (which must be an invariable quantity during the encounter) are

$$\begin{cases} (\mathbf{b}\times\mathbf{u})_x = ud\sin\theta\cos\phi \\ (\mathbf{b}\times\mathbf{u})_y = ud_p\sin\theta\cos\phi \\ (\mathbf{b}\times\mathbf{u})_z = -u(d\cos\theta + d_p\sin\theta\sin\phi). \end{cases} \tag{22}$$

The distances describing the post-encounter geometry are $d' = dk$ and $d'_p = d_p k$, where

$$k = \frac{\sin\theta\cos\phi}{\sin\theta'\cos\phi'}, \tag{23}$$

and we finally obtain the demanded quantities

$$\Omega' = \Omega + \frac{1}{a_p}[d_p - d'_p + v_p(\mathrm{d}\tau - \mathrm{d}\tau')], \tag{24}$$

$$\cos\omega' = \epsilon'_{nod}\cdot\frac{1}{e'}\left[(1-e'^2)\frac{a'}{a_p - d'} - 1\right], \tag{25}$$

$$t'_\Omega = t_\Omega + (\mathrm{d}\tau - \mathrm{d}\tau'), \tag{26}$$

where

$$\mathrm{d}\tau = \frac{1}{u}(d_p\cos\theta - d\sin\theta\sin\phi), \tag{27}$$

$$t_\Omega = t + \sqrt{a^3/G}\,(M_\Omega - M) \tag{28}$$

and t'_Ω has an homologous expression as t_Ω, but with "primed" quantities.

Because of the simplificative assumptions that we took into account, we have limits of applicability for our map. So, the condition for crossing orbits is $1 - e < a_p/a < 1 + e$ and the condition for close encounter is $r_{imp} < b < s_p$. To have an encounter near one of the nodes, we check the conditions $|d| \ll a_p$ and $|d_p| \ll a_p$ and for the validity of

the assumption about rectilinear trajectories, we impose a small value for the following quantity

$$\mathrm{d}\alpha = \sqrt{Ga(1-e^2)}\,\frac{a_p - a}{a_p^2(2a - a_p)}\,\mathrm{d}\tau, \tag{29}$$

where

$$\sin\alpha = \frac{|\mathbf{r}\times\mathbf{v}|}{rv} = \sqrt{\frac{a}{r}(1-e^2)\Big/\left(2-\frac{r}{a}\right)} \tag{30}$$

is the angle between the heliocentric position vector and velocity vector of the infinitesimal body, $\mathbf{r}$ and $\mathbf{v}$, measured near the node.

Chapter 3. Characteristics of long-term dynamical evolution

3.1 Chaotic behaviour

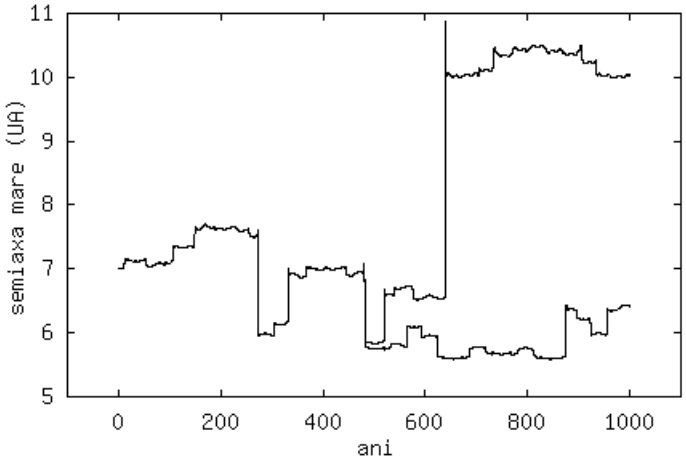

Figure 4: Semimajor axis variation of two test particles, with almost identical initial conditions, perturbed by Jupiter, in the planar, circular, restricted three-body problem. Motion is dominated by close encounters.

The phenomenon of chaos appears even in one of the simplest problems of celestial mechanics: the restricted three-body problem. Close encounters with the perturbatrice planet always induce such a chaotic behaviour for an asteroidal orbit (figure 4). But the phenomenon of chaos is more subtle, since it appears in motions totaly free of close encounters (figure 5). For the planar, circular, restricted three-body problem the Poincaré surface of section is a tool to distinguish between chaotic and regular motions. For the general case, we have the Lyapounov exponents method [Murray and Dermott, 1999], [Milani and Mazzini, 1997].

Writing the equations of motion for the n-body problem in vectorial form

$$\frac{\mathrm{d}X}{\mathrm{d}t}(t) = F(X), \tag{31}$$

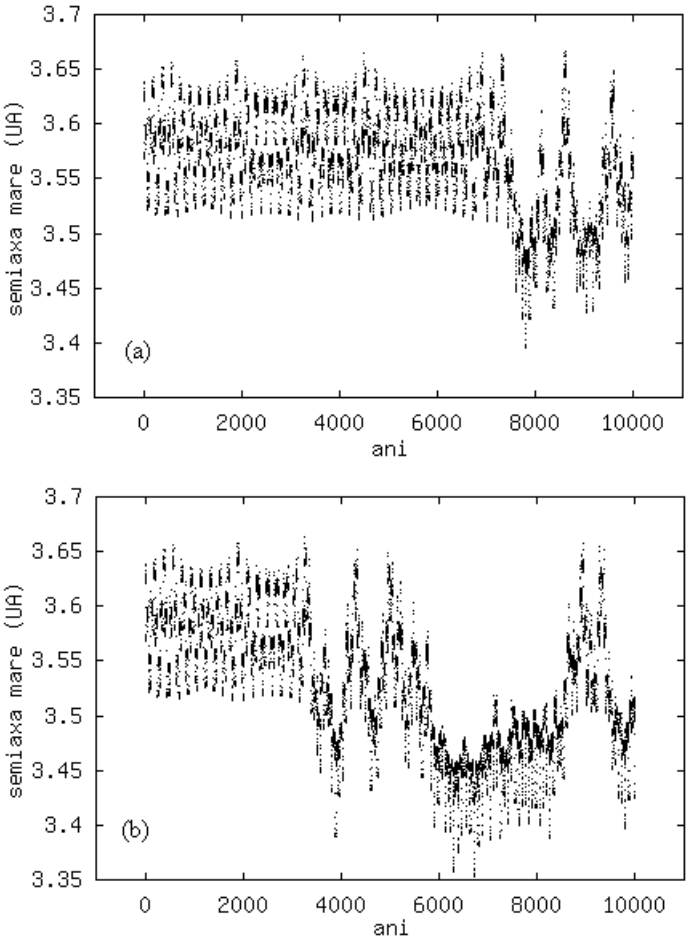

Figure 5: Semimajor axis variation of two test particles, with almost identical initial conditions, perturbed by Jupiter, in the planar, circular, restricted three-body problem. Motion is free of close encounters.

we have the integral flux $\Phi^t : X_0 \to (X(t))$ and its jacobian matrix

$$L(t) = \frac{\partial \Phi^t}{\partial X_0}(X_0), \tag{32}$$

which satisfy the variational equations

$$\frac{\mathrm{d}}{\mathrm{d}t} L(t) = \frac{\partial F}{\partial X}(X(t))L(t), \quad L(t_0) = I_6. \tag{33}$$

For a given difference in initial conditions $V(t_0) = V_0 = Y_0 - X_0$, it propagates in time as $V(t) = L(t)V_0$ (in linear approximation) and the maximum solution Λ of the limit

$$\lim_{t \to +\infty} \frac{1}{t - t_0} \ln \frac{|V(t)|}{|V_0|} = \Lambda(X_0, V_0) \tag{34}$$

defines the such called Lyapounov characteristic exponent (LCE) and the associated Lyapounov time $(1/\Lambda)$. So, we have the exponential propagation

$$V(t) = V_0 e^{\Lambda(t-t_0)}. \tag{35}$$

In the full paper we present two numerical methods for computing this exponent: first, by solving the variational equations (with or without renormalization), and second, by considering the simplest case of keplerian propagation, such as [Muller and Dvorak, 1995]

$$\Lambda = \frac{\ln(\mathrm{d}\lambda) - \ln(\mathrm{d}\lambda_0)}{t - t_0}, \tag{36}$$

where $\mathrm{d}\lambda_0$ and $\mathrm{d}\lambda$ are initial and final differences measured along the orbit. In figure 6 we present an example for this method.

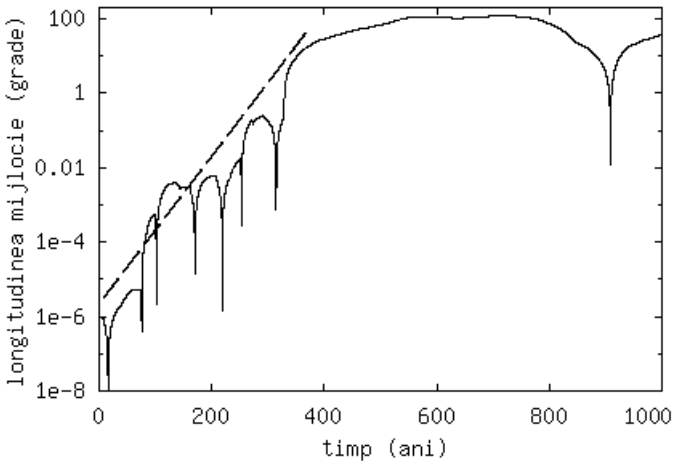

Figure 6: Numerical estimation of the LCE of asteroid (1862) Apollo, by monitoring the accumulated difference in mean longitude $\mathrm{d}\lambda$ between the asteroid and a "virtual image" of it (the computed Lyapounov time is about 25 years).

The effect of chaos on long-term numerical integrations is discussed. In summary, the exponential divergence in time of the specific three types of errors (error in initial conditions, approximation error and round-off error) limits the deterministic nature of the final numerical solution.

3.2 Resonant motions

Starting with the mean motion resonances, we consider the geometric and the dynamical interpretation of this phenomenon, characterized by the libration of the resonant argument (in standard notations)

$$\sigma_{p:q} = p\lambda_p - q\lambda - (p-q)\varpi, \tag{37}$$

for a given p/q resonance ratio. Figure 7 presents a real example of a capture in resonance.

Next, we give a method for identifying resonant motions by developing the irrational number [Janiczek *et al.*, 1972]

$$r = \left(\frac{a_p}{a}\right)^{3/2} \tag{38}$$

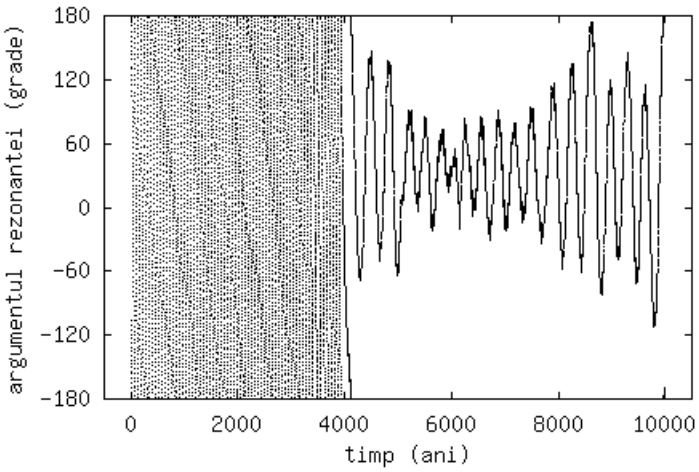

Figure 7: Variation of the resonant argument $\sigma_{10:3}$ for the asteroid (4197) 1982 TA in respect to Jupiter. The transition between circulation and libration shows that the asteroid is captured in 10:3 mean motion resonance.

in continuous fraction, in order to obtain a resonance ratio p/q and to test if indeed the corresponding resonant argument librates.

The secular resonances ν_5 ($\dot{\varpi} \approx \dot{\varpi}_J$), ν_6 ($\dot{\varpi} \approx \dot{\varpi}_S$), ν_{16} ($\dot{\Omega} \approx \dot{\Omega}_S$), and Kozai ($\dot{\omega} = 0$, $K = \sqrt{1-e^2}\cos I$) are summarized [Froeschlé and Morbidelli, 1994] and the fundamental frequencies of Jupiter and Saturn (listed above with indices J and S) are numerically computed.

A common characteristic of NEA crossing orbits is their translation along the Tisserand contours in respect to Earth, allowing many close encounters to take place in time. But there are also exceptions to this rule, i.e. bodies which are protected against close encounters by some kind of protection mechanisms. These mechanisms are described in the paper, such as: mean motion resonances, or motions around stable Lagrange equilibrium points, or the Kozai secular resonance (some examples are given in figures 8 and 9 below).

3.3 Dynamical classifications

First of all, we give here classifications against MOID, computed in respect to Earth's orbit. We have, for instance, the such called potentially hazardous asteroids (PHA), situated on orbits for which this distance is smaller than 0.05 UA. Another classification, with more deep implications, is proposed by the author [Berinde, 1999b]. After extensive numerical integrations of NEAs orbits, we have identified three types of dynamical behaviours of the MOID: short-time orbital approach, periodic orbital approach and long-time orbital approach (figure 10).

At the end of this chapter we analyze the SPACEGUARD classification of the NEA population, describing the following classes: Toro, Kozai, Geographos, Eros, Alinda and Oljato [Milani, 1998].

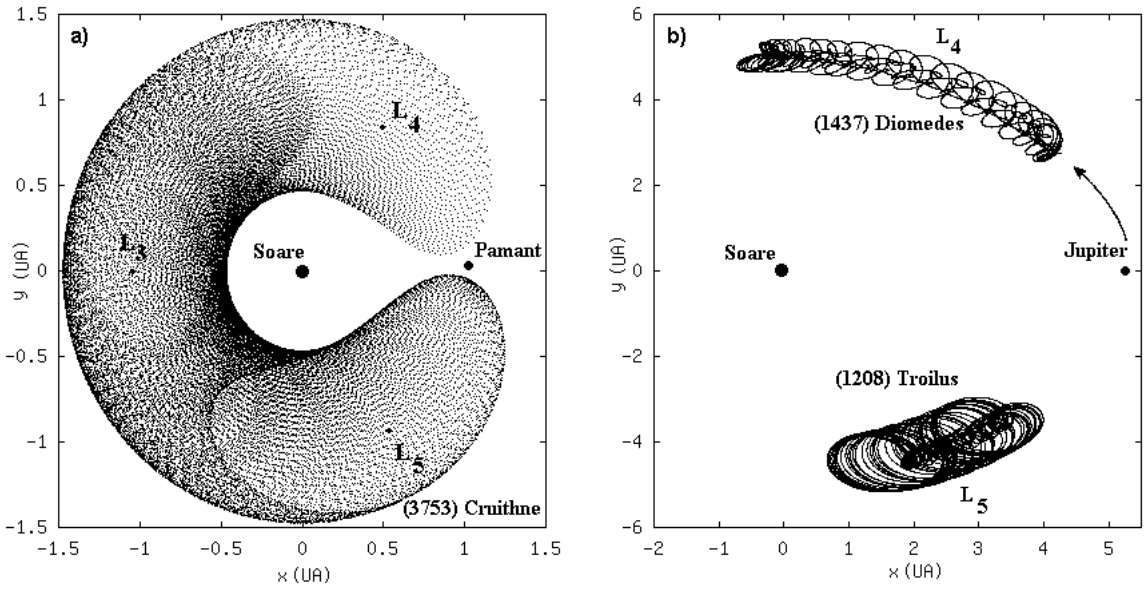

Figure 8: a). Dynamical evolution of asteroid (3753) Cruithne on a horseshoe-like orbit in respect to Earth; b). Dynamical evolutions of two trojan asteroids, (1437) Diomedes and (1208) Troilus, on tadpole-like orbits in respect to Jupiter (no example for Earth). All these motions are represented in corotational frames for 500 years. No close encounters take place.

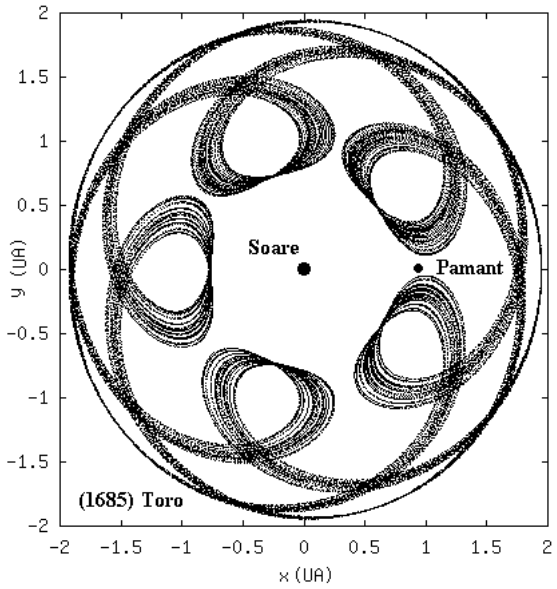

Figure 9: Dynamical evolution of asteroid (1685) Toro in 5:8 mean motion resonance with Earth. Motion is represented in a corotational frame for 1000 years. No close encounters take place.

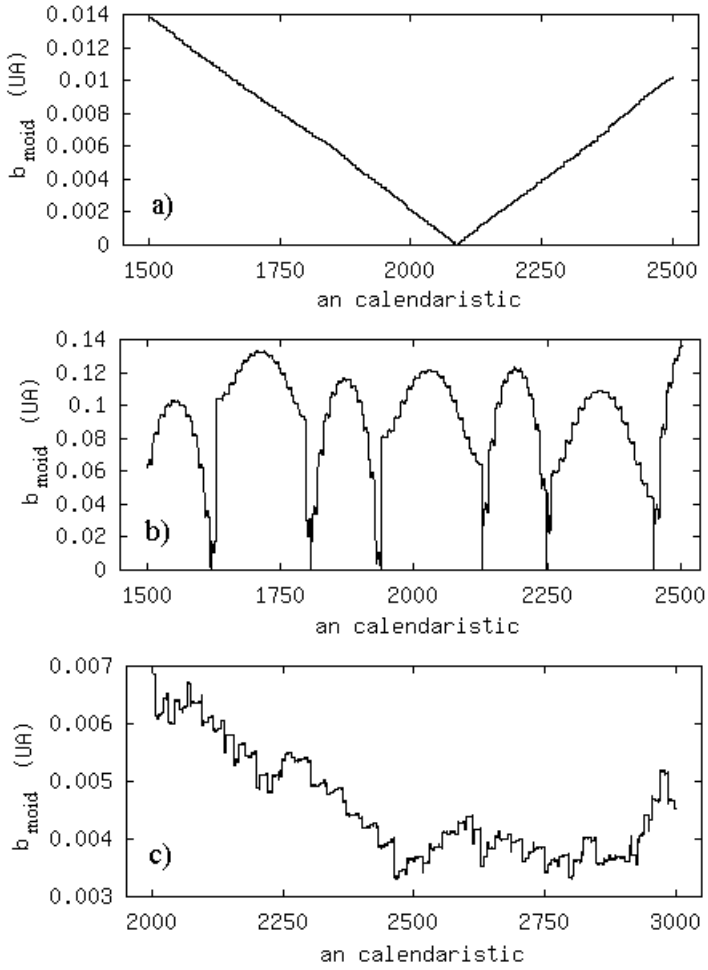

Figure 10: Three types of dynamical behaviours of the MOID, computed for one thousand years: a) short-time orbital approach - the asteroid 2000 WO_{107}; b) periodic orbital approach - the asteroid (1915) Quetzalcoatl; c) long-time orbital approach - the asteroid 1999 MN.

Chapter 4. Source regions and dynamical transport mechanisms

4.1 The main belt of asteroids as NEA source

In the first part of the chapter we discuss about the dynamical structure of the main belt, which is strongly modeled by several mean motion and secular resonances with Jupiter and Saturn, a by-product of these being the well known Kirkwood gaps. In the phase space of orbital elements, the locations of these resonances correspond to weak-populated regions, characterized by high values of the LCE (they are chaotic regions). Figure 11 shows the dynamical evolution of an asteroid located in such a chaotic region, undergoing large fluctuations in eccentricity. It becomes a NEA in about 10^5 years.

The main evolutionary paths towards the Earth's orbit are summarized on figure 12. Fast-tracks and slow-tracks are highlighted, together with their associated dynamical life-times [Greenberg and Nolan, 1993]. The most effective resonances in delivering asteroidal

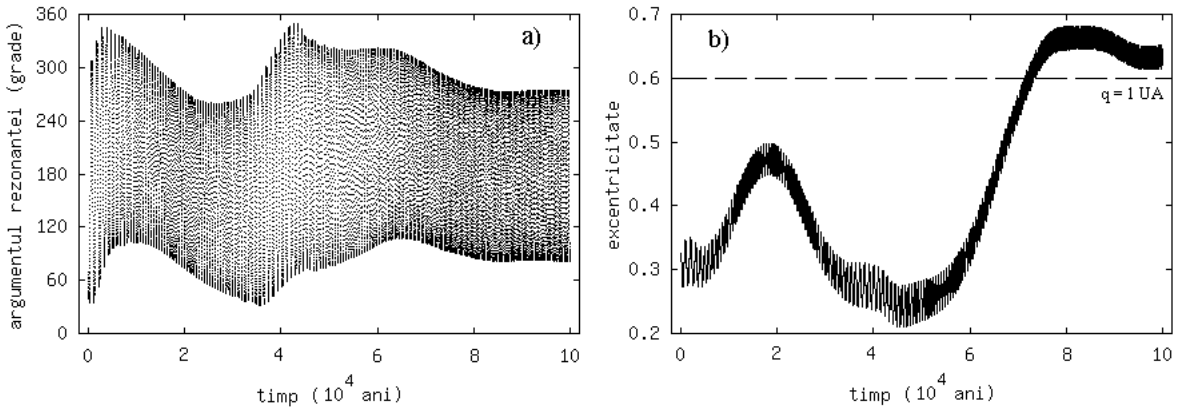

Figure 11: Dynamical evolution of a fictitious asteroid placed in 3:1 mean motion resonance with Jupiter, having the following keplerian elements at the initial epoch JD 2451545.0: $a = 2.4893663$ UA, $e = 0.326086$, $I = 5^\circ.34915$, $\Omega = 0^\circ$, $\omega = 0^\circ$ and $M = 33^\circ.2367$. The dynamical system in which this integration was performed is Sun−the four giant planets−asteroid. a) variation of the resonant argument $\sigma_{3:1}$ and b) variation of the eccentricity.

fragments are 3:1, 4:1 and ν_{16}.

The inter-asteroidal collision seems to be an efficient mechanism to supply with material the chaotic regions described above, by changing the semimajor axis of collisional fragments with at least 0.03 UA. In order to study the effectiveness of this process, we start with laboratory experiments on collisions.

After defining several types of collisions [Fujiwara *et al.*, 1989], we present some models about the distribution of mass and velocity in the ejecta, like

-the power law distribution of fragments' cumulative number, in term of their mass m (or radius r)

$$N(>m) = A\, m^{-\alpha}, \quad N(>r) = B\, r^{-\beta}, \tag{39}$$

-the cumulative model of mass distribution, function of the ejection velocity

$$m(>v) = \begin{cases} M_t \left(\dfrac{v}{v_0}\right)^{-k} & , v \geq v_0 \\ \\ M_t & , v < v_0, \end{cases} \tag{40}$$

where M_t is the mass of the largest fragment, animated by the smallest ejection velocity v_0,

-the distribution of fragments' number, function of their ejection velocity

$$\mathrm{d}N(v) = \begin{cases} C\, v^{-(k+1)} & , v \geq v_0 \\ 0 & , v < v_0, \end{cases} \tag{41}$$

and so on.

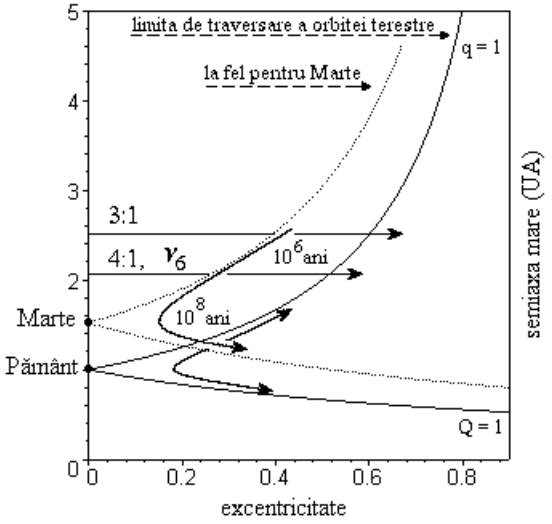

Figure 12: The evolutionary paths of main belt asteroids towards the Earth's orbit and the associated mean delivery lifetimes, represented in the plane of orbital elements (e, a).

By scaling the laboratory results at the real size of an inter-asteroidal collision and taking into account the gravitational field of the target, we have the following relations [Farinella *et al.*, 1994]

-the distribution of fragments' number, function of their final velocity

$$\mathrm{d}N(v_\infty) = \begin{cases} C'\, v_\infty (v_\infty^2 + v_{par}^2)^{-(k+2)/2}\, \mathrm{d}v_\infty & , v_\infty^2 \geq v_0^2 - v_{par}^2 \\ \\ 0 & , v_\infty^2 < v_0^2 - v_{par}^2, \end{cases} \tag{42}$$

where v_{par} is the escape velocity,

-the number of collisional fragments escaping at infinity, function of the target radius R

$$N(v > v_{par}) = \int_{v_{par}}^{\infty} C v^{-(k+1)} \mathrm{d}v \sim \left(\frac{R}{R_0}\right)^{-k}, \tag{43}$$

where R_0 is the minimum radius for which all fragments reaccumulate on the surface of the target.

Adopting a theoretical model for the following processes: the catastrophic collision (with fragmentation) and the cratering collision, we can evaluate the mass of the ejecta in each case, and their corresponding ratio

$$\frac{M_{cra}}{M_{cat}} = \frac{\beta\gamma}{3-\beta}, \tag{44}$$

showing that the efficiency of one type of collision against the other one depends on the exponent β (γ being a constant). We consider some theoretical interpretations of β-values, invoking the such called collisional equilibrium model [Greenberg and Nolan, 1989]. We obtain the following values characterizing the collisional fragments in equilibrium $\beta_{equ} =$

5/2, and the fresh delivered collisional fragments in resonances $\beta_{exp} = 3$. These values are then compared with the observed ones, for the unbiased NEA population [Rabinowitz *et al.*, 1994]

$$\beta = \begin{cases} 3.5, & 10 \text{ m} < D < 70 \text{ m} \\ 2.0, & 70 \text{ m} < D < 3.5 \text{ km} \\ 5.4, & D > 3.5 \text{ km}. \end{cases} \tag{45}$$

where D denotes the diameter of the object.

A short overview on Yarkovsky effect is also given.

Next, we pay attention on obtaining a rough estimation for the asteroids' mass, using for this the photometric model based on the well known H-G magnitude system described in [Bowell *et al.*, 1989]. It evaluates the diameter of the body function of its absolute magnitude H, its geometric albedo p and the Sun magnitude in a certain observing domain $m_\odot$,

$$D = \frac{2}{\sqrt{p}}\, 10^{(m_\odot - H)/5}, \tag{46}$$

and for a spherical body we get the mass

$$\begin{aligned} M &= 1.3 \times 10^{21-3H/5}\, \rho p^{-3/2} \text{ [kg]} \\ &= 6.5 \times 10^{-(10+3H/5)}\, \rho p^{-3/2} \text{ [}M_\odot\text{]}, \end{aligned} \tag{47}$$

where ρ is the density.

4.2 NEA asteroids of cometary origin

We begin this section by presenting various populations of bodies from the other solar system, which might be related to the NEA population of cometary origin (figure 13): Jupiter-family comets, Halley-type comets, Centaurus objects and trans-neptunian objects. As a part of this study, we propose a model of chaotic diffusion of trans-neptunian objects to the inner solar system, based on the complete map of orbital changes developed in chapter 2 [Berinde, 2001a].

Planet	Collision	Hyperbolic or parabolic orbit
Jupiter	15.5	27.0
Saturn	4.1	25.0
Uranus	1.1	5.9
Neptune	1.9	19.6
-total-	22.5 %	77.4 %

Table 1: The percent of evolutionary end-states, function of the giant planet involved on it.

We start with an initial population of bodies in Neptune-crossing orbits (figure 13) which are animated by a synthetic secular drift, $\omega = \omega_0 + \mathrm{d}\omega\, t$ and $\Omega = \Omega_0 - \mathrm{d}\Omega\, t$, accor-

dingly with the results of some numerical experiments. By following 4000 samples through multiple close encounters with the giant planets, for their entire dynamical history, we have obtained a statistical pictures of this impressive scattering process.

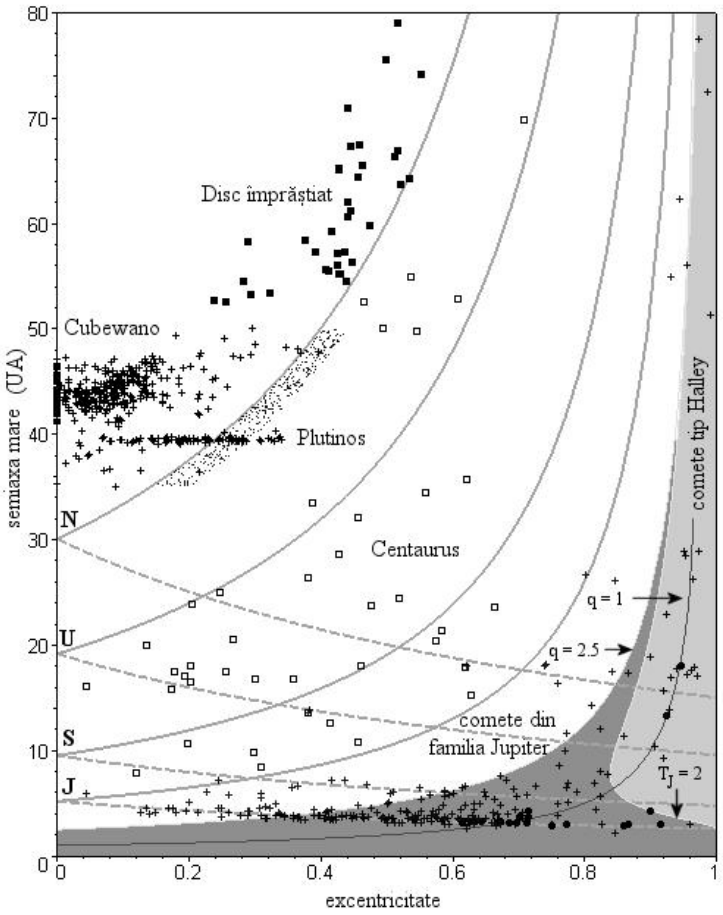

Figure 13: Discovered populations of bodies in the outer solar system, represented in the plane of orbital elements (e, a). We have: several NEA asteroids on cometary-like orbits - through filled circles, the population of short-period comets (Jupiter-family ones and Halley-type ones) - through crosses, Centaurus population - through empty squares, the trans-neptunian population (with the sub-populations Cubewano and Plutinos - also through crosses, scattered disk population - through filled squares), and a virtual population of bodies on Neptune-crossing orbits (subject of the simulation) - through dots. We depicted also the Tisserand contours corresponding to distances at perihelion and aphelion of the body's orbit matching the planetary semimajor axes (J-Jupiter, S-Saturn, etc) and the contours $q = 1$ UA, $q = 2.5$ UA and $T_J = 2$.

The dynamical evolution of one body randomly choosen from our simulation is shown on figure 14. Its existence ceases after 130 My through a collision with Jupiter. Accumulating all information from the entire population, we have mapped on (a, e) plane the frequency of close encounters with the giant planets (figure 15).

The evolutionary end-states are summarized on table 1. Also, some dynamical lifetimes are indicated in the full paper. We evaluate about 42% from the initial population will

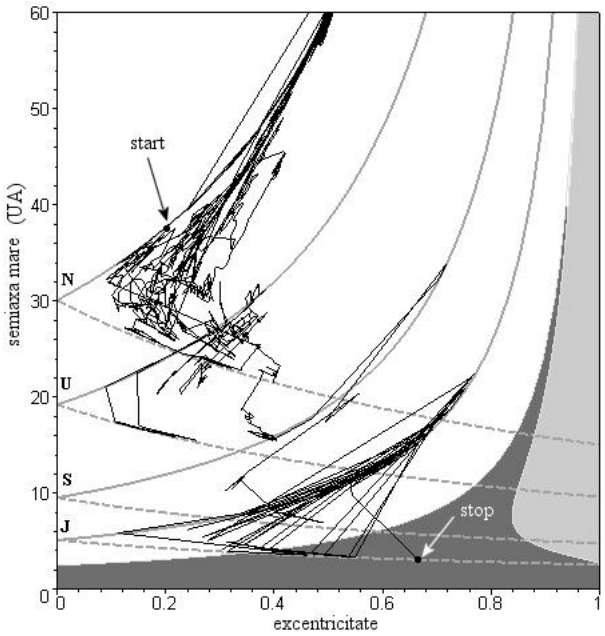

Figure 14: The evolutionary path of a fictitious Neptune-crossing body throughout the outer solar system. We depicted also the Tisserand contours corresponding to distances at perihelion and aphelion of the body's orbit matching the planetary semimajor axes (J-Jupiter, S-Saturn, etc).

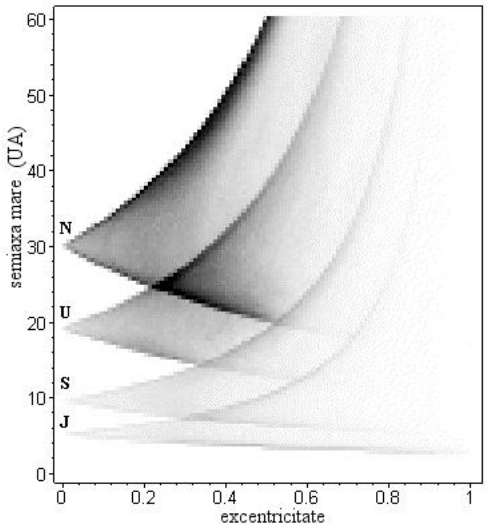

Figure 15: A gray composition showing the cumulative number of close encounters with the giant planets, distributed over the (e, a) plane of orbital elements, for the entire simulated population. Dark nuances proportionally correspond at larger numbers.

enter into the such called active cometary region ($q < 1.5$ UA), becoming an active short-period comet.

Chapter 5. Methods of estimating the impact probability with the Earth

5.1 Mean impact probabilities

These are probabilities derived when a simplified model of motion is supposed to be valid, like the hypothesis of random variation of some angular orbital elements, or the invariability of the flux of passages through the cross-section of unity area.

First method is based on counting the number of close encounters $N(d)$ taking place at various distances d from the planet, in a certain interval of time, and extrapolating the result at the surface of the planet [Sekanina and Yeomans, 1984]. The following theoretical relation holds, involving the desired number of collisions N_c

$$\frac{N(d)}{N_c} = \left(\frac{d}{R_p}\right)^2 \left[\frac{1+\frac{R_p}{d}\left(\frac{v_{par}}{\bar{u}}\right)^2}{1+\left(\frac{v_{par}}{\bar{u}}\right)^2}\right], \tag{48}$$

but the extrapolation can be made linearly in a log-log plot through

$$\mathbf{D}: \quad \lg N(d) = A + 2\lg\left(\frac{d}{R_p}\right), \tag{49}$$

or using the following curve

$$\mathbf{C}: \quad \lg N(d) = A_1 + A_2 \lg\left(\frac{d}{R_p}\right) + \lg\left[1+\left(\frac{v_{par}}{\bar{u}}\right)^2 10^{-\lg\left(\frac{d}{R_p}\right)}\right], \tag{50}$$

which includes the gravitational focusing of the planet. Here $\bar{u}$ is the mean unperturbed planetocentric velocity of the asteroid at various close encounters, R_p is the radius of the planet and v_{par} is the escape velocity on its surface. A, A_1 and A_2 are parameters to be fitted. Examples are given for two asteroids on next figure, after integrating their motion for 10^5 years.

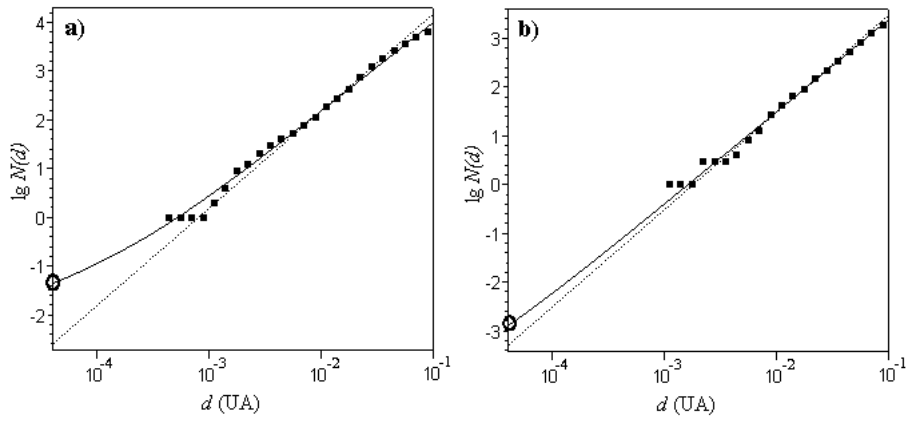

Figure 16: Extrapolating the mean impact probability with the Earth for the asteroids a) 2000 SG_{344} and b) 1999 AN_{10}. Dotted line shows the linear extrapolation and continuous line shows the extrapolation on curve.

The second method from this section is based on the paper [Steel and Baggaley, 1985]. The impact probability is expressed as

$$P = \int_{\mathcal{V}} s_1 s_2 \, u\sigma \, \mathrm{d}\nu, \tag{51}$$

where $\mathcal{V}$ is the volume of space in which the encountering bodies may collide. It depends on the collision cross-section σ and on the spatial densities of the bodies s_1 and s_2. These quantities can be evaluated analytically, function of two variables (r, β), namely the distance to primary and the ecliptic latitude, such as

$$s(r,\beta) = \frac{1}{2\pi^3 r a \sqrt{(\sin^2 I - \sin^2 \beta)(r-q)(Q-r)}}. \tag{52}$$

In order to avoid the singularities arising near aphelion and perihelion, this expression is averaged as follows

$$\begin{aligned} \bar{s}(r,r',\beta,\beta') = & \frac{1}{2\pi^3 a \bar{r} \Delta r (\sin\beta' - \sin\beta)} \left[\arcsin\left(\frac{2r'-2a}{Q-q}\right) - \arcsin\left(\frac{2r-2a}{Q-q}\right) \right] \cdot \\ & \left[\arcsin\left(\frac{\sin\beta'}{\sin I}\right) - \arcsin\left(\frac{\sin\beta}{\sin I}\right) \right], \end{aligned} \tag{53}$$

on the infinitesimal elements ΔR and $\Delta\beta$.

For the circular case of the planetary orbit, the spatial density of the asteroid is simply given by

$$\bar{s} = \frac{1}{2\pi^3 a_p \, a \sin I \sqrt{(a_p - q)(Q - a_p)}}, \tag{54}$$

where the radius a_p of the circular orbit is involved here.

We exemplify this method on the entire population of discovered ECAs (figure 17).

5.2 Intrinsic impact probabilities

The method of computing the intrinsic impact probability is described and widely commented in a series of recent papers by [Milani, 1999], [Milani and Valsecchi, 1999], [Milani *et al.*, 2000a], [Milani *et al.*, 2000b] etc. It consists in defining the initial uncertainty region of an asteroid, its propagation in time, its projection on the target plane of a given close encounter and, finally, in identifying the virtual impactors and computing the intrinsic impact probability.

The starting point is the theory of orbit determination from a set of observational data, with the following residuals in right ascension and declination

$$\left\{ \begin{array}{rcll} \xi_{2k-1} = & w_{2k-1} \cdot [\alpha_k^o - \alpha^c(t_k)] \cos\delta_k^o & \\ \xi_{2k} = & w_{2k} \cdot [\delta_k^o - \delta^c(t_k)], & k = \overline{1,n} \end{array} \right. \tag{55}$$

which are supposed to follow a gaussian distribution

$$P(\xi_1, \xi_2, \ldots, \xi_{2n}) \propto e^{-\frac{1}{2}\xi^T W^{-1} \xi} \tag{56}$$

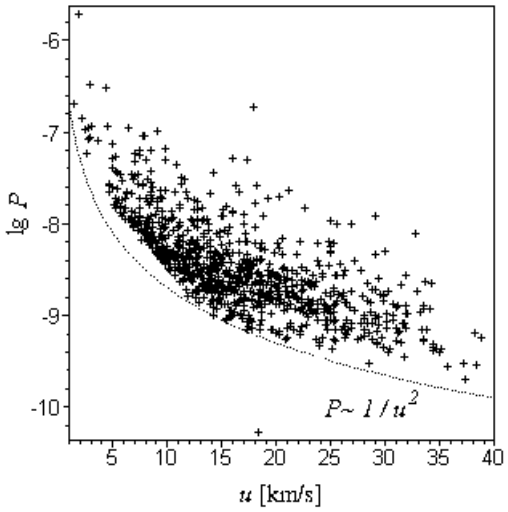

Figure 17: Annual mean impact probabilities with the Earth for the entire population of discovered ECAs (more than 900 objects), function of their impact velocities. A tendency in this distribution is highlighted.

around the nominal orbit E^*, which is the solution of the least square method for the target function

$$Q(E) = \xi_1^2 + \xi_2^2 + \cdots + \xi_{2n}^2. \tag{57}$$

The uncertainty region is defined by the inequality

$$\delta Q(E) = Q(E) - Q(E^*) \leq \sigma^2 \tag{58}$$

and, in linear approximation, by the uncertainty ellipsoid

$$\delta Q(E) \approx \delta E \, N \, \delta E^T \leq \sigma^2, \tag{59}$$

where N is the normal matrix.

The transformation of the uncertainty ellipsoid when changing the coordinate system is considered

$$\delta E' \, N' \, (\delta E')^T = \delta E \left(\frac{\partial E'}{\partial E} \right)^T N' \left(\frac{\partial E'}{\partial E} \right) \delta E^T = \delta E \, N \, \delta E^T \leq \sigma^2, \tag{60}$$

especially for computing its canonical form

$$\frac{1}{\lambda_1} \delta e'^2_1 + \cdots + \frac{1}{\lambda_6} \delta e'^2_6 \leq \sigma^2, \tag{61}$$

and its image in the tridimensional space of motion (figure 18).

Afterwards, the propagation of the orbital uncertainty region is studied, in various approximations, namely in the frame of two-, three- and n-body problem.

The importance of the line of variation (LOV) in the frame of two-body problem is highlighted. It describes the uncertainty along the orbit

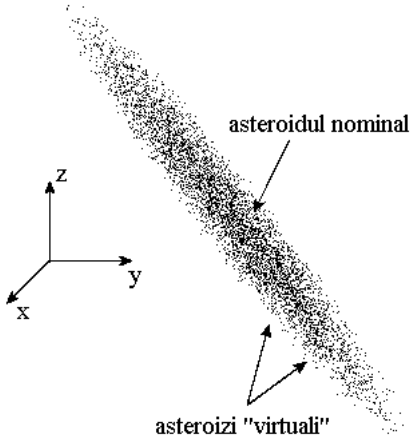

Figure 18: The image of the uncertainty ellipsoid in the tridimensional space of motion.

$$\delta\lambda \approx \pm \left[\delta\lambda_0 + \frac{3}{2}\sqrt{G} a_0^{-5/2} (t - t_0)\, \delta a_0 \right], \tag{62}$$

.

In the frame of circular, restricted three-body problem, the propagation of the uncertainty region is the contribution of the author [Berinde, 2001b]. Using the Öpik's formalism, it is possible to evaluate through analytical formulas the dispersion of the orbital elements during a close encounter, especially the dispersion of the semimajor axis

$$a' = a_p / \left[1 - 2 \left(\frac{u}{v_p} \right) \cos\theta' - \left(\frac{u}{v_p} \right)^2 \right] \tag{63}$$

is useful

$$\delta a' = C_1 \left(\frac{a'}{b} \right) \left[C_2 \left(\frac{R_p}{b} \right) + C_3 \left(\frac{b_{\text{moid}}}{b} \right)^2 \right] \delta M. \tag{64}$$

The coefficients

$$\begin{cases} C_1 = 2a' \left(\dfrac{a}{a_p} \right)^{3/2} \left(\dfrac{u}{v_p} \right) \sin\theta \\ C_2 = \left(\dfrac{v_{\text{par}}}{u} \right)^2 (\cos\theta \sin\gamma - \sin\theta \cos\gamma \cos\psi) \cos\psi \\ C_3 = \sin\theta \sin\gamma \end{cases} \tag{65}$$

are of the order of unity. We are able to evaluate at this point the magnitude of the dispersion $\delta a' \approx (10^{-1} - 10^4) \cdot \delta M$ [UA], function of the encounter's geometry and of the initial uncertainty along the orbit δM. On the other hand, an oscillatory behaviour in δM is identified and explained (see figure 19), having the role of keeping at small values the orbital uncertainty.

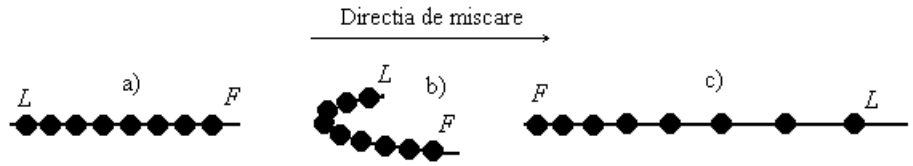

Figure 19: The rearrangement process of virtual asteroids along the direction of motion (F denotes the first asteroid in the string and L the last one).

In essence, this behaviour depends on the sign of $\delta a'$, with the following extreme cases written in terms of the encounter parameter b and of the MOID value, b_{moid}, namely $b \approx b_{\text{moid}}$ ($\mathrm{d}a' > 0$) and $b \gg b_{\text{moid}}$ ($\mathrm{d}a' < 0$). A real example of such behaviour is shown on figure 20.

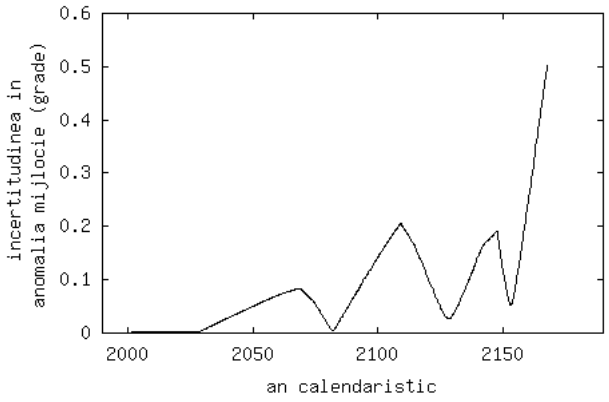

Figure 20: The oscillatory behaviour of the uncertainty in mean anomaly for the asteroid 1999 AN_{10}, obtained by numerically integrating a set of 100 virtual asteroids uniformly distributed in the initial uncertainty region, for $\sigma = 1$.

Limits of applicability of the linear propagation theory are discussed (see figure 21). Some alternative semi-analytical and numerical methods are briefly suggested, but we pay an extensive attention to the Monte-Carlo sampling technique.

The such called b-plane and modified target plane (MTP) are introduced and the problem of identifying and cataloging close encounters is also discussed. After this, some linear approximations for the impact probability

$$\mathcal{P}_{imp} = \int_{\mathcal{C}_E} P_0(E)\,\mathrm{d}E \tag{66}$$

are summarized. This integral in evaluated on the subspace $\mathcal{C}_E$ leading to collisional trajectories, situated in the initial uncertainty region $\mathcal{E}_0$, where the orbital elements are distributed in accordance with P_0. Its expression can be rewritten in a suitable form using a coordinate system $(\sigma_\Lambda, \sigma_w)$ on the target plane, as

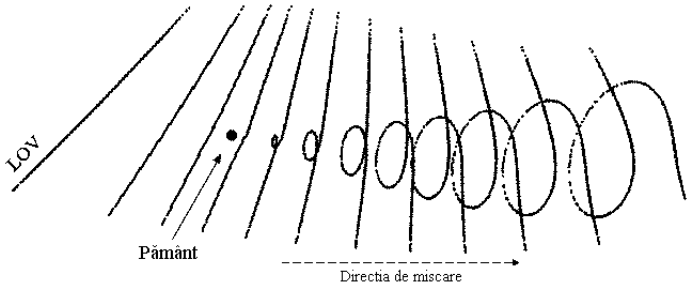

Figure 21: Monte-Carlo propagation of the uncertainty region of the asteroid 2001 GP_2 in the tridimensional space of motion, during a close encounter with the Earth (minimum distance Earth - LOV: 0.0013 UA, on October 5, 2020). The nonlinear character of propagation after the encounter is pointed out.

$$\mathcal{P}_{imp} = \int_{\mathcal{E}_T \cap \mathcal{R}_p} \frac{P_\sigma(\sigma_\Lambda) P_\sigma(\sigma_w)}{\Lambda w} \, \mathrm{d}\tau, \tag{67}$$

where $\mathcal{E}_T$ is the uncertainty ellipse and $\mathcal{R}_p$ is the image of the Earth on that plane. Some analytical solutions for this integral are derived in certain cases.

When we speak about the numerical evaluation of the impact probability (67), we refer to the Monte-Carlo sampling technique. The fundamental theory behind this method is presented [Press *et al.*, 1997].

Based on it, we propose an iterative Monte-Carlo algorithm for finding virtual impactors for a given close encounter, by propagating on several steps a limited number of virtual asteroids. This numerical simulation is accompanied by a topologic analysis performed on the target plane and also in the initial uncertainty region. The following set of initial orbits $(E_1, E_2, \ldots, E_N)$ is propagated on the target plane in $(T_1, T_2, \ldots, T_N)$. We suppose these points are already ordered by their distance to the planet center, so that $d_1 \leq d_2 \leq \cdots \leq d_N$. We consider the following set of points

$$M = \{T_2\} \cup \{T_i |\ d_i \leq R_p, i = \overline{3, N}\} \cup \{T_j |\ \rho_{1j} \leq d_1, j = \overline{3, N}\}, \tag{68}$$

where ρ_{ij} is the distance between the points T_i and T_j. We compute the following radius $r = \max\{||E - E_1||,\ E \in M^{-1}\}$ using the Chebyshev metric, where M^{-1} is the image of M in the initial uncertainty region. We build the six-dimensional hypercube $H(E_1, r) = \{E \in \mathbb{R}^6,\ ||E - E_1|| \leq r\}$, which gives the next region to be sampled $S = H(E_1, r) \cap \mathcal{E}_0$. After n iteration steps, the region S^n bounds as closely as possible the set of virtual impactors around the closest one E^n, and we estimate

$$\mathcal{P}_{imp} = \frac{k}{N} \int_{S^n} P_0(E) \, \mathrm{d}E, \tag{69}$$

where k is the number of identified virtual impactors.

We distinguish the following particular cases with analytic solutions:

-when $r_n \ll \min\{\sigma\sqrt{\lambda_1}, \ldots, \sigma\sqrt{\lambda_6}\}$,

$$\mathcal{P}_{imp} = (2r_n)^6 \frac{k}{N} P_0(E^n), \tag{70}$$

-when $\lambda_6 \gg \max\{\lambda_1, \ldots, \lambda_5\}$,

$$\mathcal{P}_{imp} = \frac{k}{N} \int_{\lambda}^{\lambda'} P_0(\lambda)\, \mathrm{d}\lambda \equiv \frac{k}{N} \frac{r_n}{\sigma\sqrt{\lambda_1}}. \tag{71}$$

The convergence of the method and its applicability are discussed.

Examples are given for the asteroids 2000 SG_{344} and 2001 BA_{16} (table 2). In figure 22 we sketch how this method works, by showing the discrete images of the uncertainty region on the target plane.

Asteroid name	2000 SG_{344}	2001 BA_{16}
Number of iterations	$n = 2$	$n = 3$
Identified impactors	$k = 9$	$k = 10$
Orbital elements of the closest virtual impactor at the initial epoch 2001 Oct. 18.00 UT (JD 2452200.5)	$a = 0.9776044188$ UA $e = 0.0669830990$ $I = 0°.10934932$ $\Omega = 192°.53703809$ $\omega = 274°.61406671$ $M = 300°.46664608$	$a = 0.9404420998$ UA $e = 0.1370062676$ $I = 5°.75614065$ $\Omega = 115°.64065318$ $\omega = 242°.81635947$ $M = 40°.17319347$
Minimum distance of impact	0.16 (terrestrial radii)	0.54 (terrestrial radii)
$\int_{S^n} P_0(E)\, \mathrm{d}E$	$3 \cdot 10^{-3} \pm 2\%$	$7 \cdot 10^{-5} \pm 3\%$
Date of the event	2071 Sep. 16.05 UT (JD 2477735.55)	2041 Jan. 15.06 UT (JD 2466534.56)
Impact probability	$\approx 5 \cdot 10^{-5}$	$\approx 10^{-6}$

Table 2: Relevant parameters in computing the impact probabilities with the Earth for the asteroids 2000 SG_{344} and 2001 BA_{16}, during two close encounter for which virtual impactors have been identified.

5.3 Quantifying the impact hazard

The Torino [Binzel, 1997] and Palermo scales [Chesley *et al.*, 2001] are presented, as tools for quantifying the impact hazard in terms of impact probability, impact energy and warning time. Examples on computing the impact hazard on Palermo scale are summarized on table 4. Here, v is the impact velocity, d is a rough estimation of the asteroid's diameter, E is the impact energy, f_B is the annual mean impact frequency for the entire population of NEAs, having an impact energy greater than E, ΔT is the interval of time in which the probability P is computed, R is the such called normalized risk and $\mathcal{P}$ is the Palermo hazard index.

The consequences of the impact phenomenon on Earth are also considered [Hills and Goda, 1993]:

-the diameter of the devastated area due to the shock wave propagation of an explosion in the atmosphere

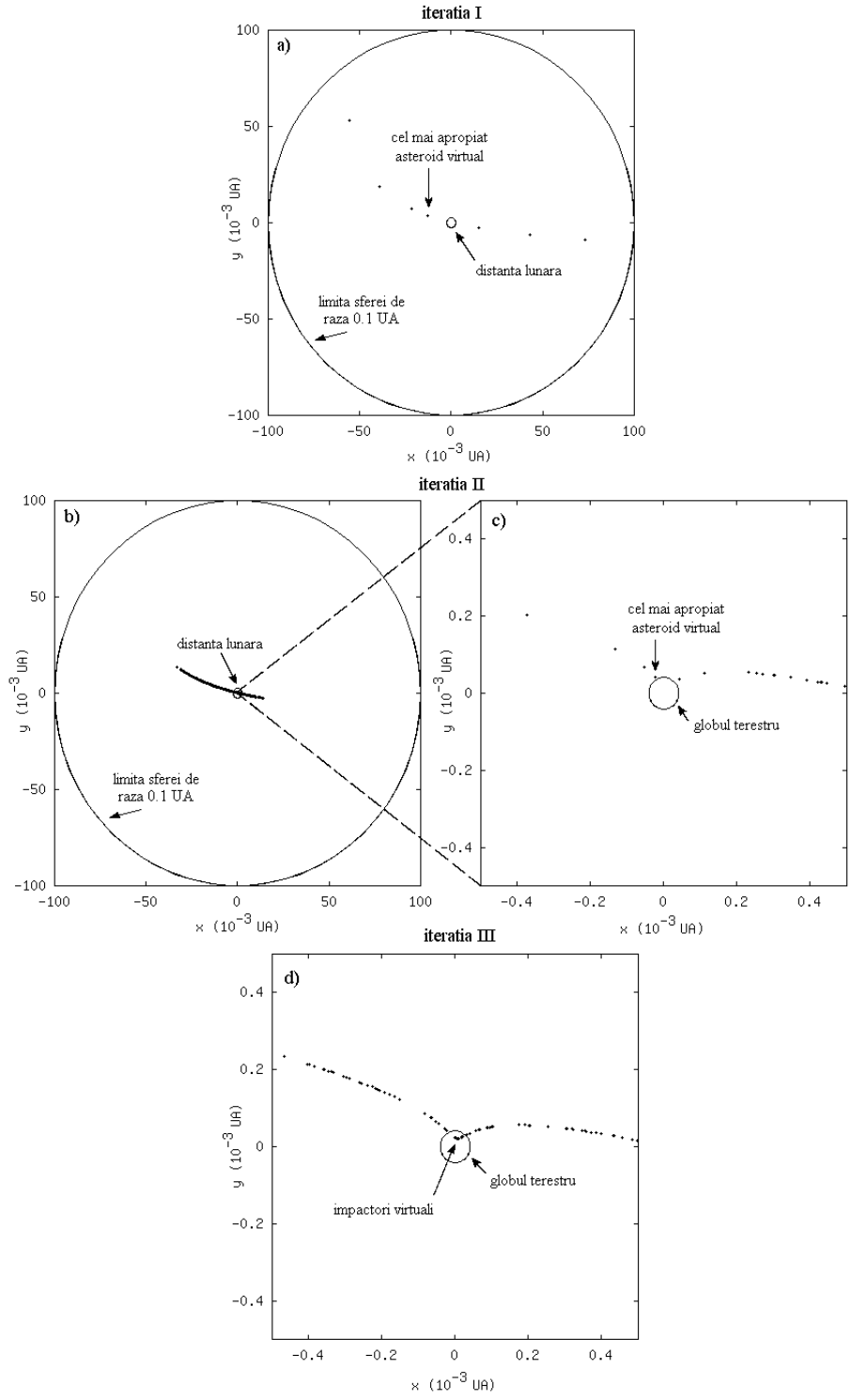

Figure 22: The images of uncertainty region projected on the target plane, for the asteroid 2000 BA_{16}, during three iterations of the Monte-Carlo method for finding virtual impactors.

Object	v (km/s)	d (m)	E (Mt)	f_B (/year)	ΔT (years)	P	$\mathcal{R}$	$\mathcal{P}$
2000 SG_{344}	11.34	40	1.1	2.8×10^{-2}	100	5×10^{-5}	1.8×10^{-5}	-4.7
2000 SG_{344} †	11.34	40	1.1	2.8×10^{-2}	10^5	4.4×10^{-2}	1.6×10^{-5}	-4.8
2001 BA_{16}	12.14	20	0.3	7.9×10^{-2}	50	10^{-6}	2.5×10^{-7}	-6.6

Table 3: Relevant parameters in computing the hazard index on Palermo scale for the asteroids 2000 SG_{344} and 2001 BA_{16}. († in this case the parameters are computed for the extrapolated probability from the frequency of close encounters with the Earth, in 100.000 years of integration time).

$$D_e \approx 15.8 \text{ km} \left(\frac{d}{100 \text{ m}}\right) \left(\frac{\rho}{3 \text{ g/cm}^3}\right)^{1/3} \left(\frac{v}{20 \text{ km/s}}\right)^{2/3}, \tag{72}$$

-the diameter of the impact crater

$$D_c \approx 4.3 \text{ km} \left(\frac{d}{100 \text{ m}}\right) \left(\frac{\rho}{3 \text{ g/cm}^3}\right)^{1/3} \left(\frac{v}{20 \text{ km/s}}\right)^{2/3}, \tag{73}$$

-the magnitude of the earthquake produced by an impact on land (Richter scale)

$$M \approx 7.3 + 2.1 \lg \left(\frac{d}{100 \text{ m}}\right) + 0.7 \lg \left(\frac{\rho}{3 \text{ g/cm}^3}\right) + 1.4 \lg \left(\frac{v}{20 \text{ km/s}}\right), \tag{74}$$

-the height of the oceanic wave produced by an impact on water

$$H_w \approx 16.2 \text{ m} \left(\frac{1000 \text{ km}}{r}\right) \left[\left(\frac{d}{100 \text{ m}}\right)^3 \left(\frac{\rho}{3 \text{ g/cm}^3}\right) \left(\frac{v}{20 \text{ km/s}}\right)^2\right]^{0.54}, \tag{75}$$

where d is the diameter of the projectile, ρ is the density, v is the impact velocity and r is the distance from the wave to the impact center. Mean values for these quantities are considered in corresponding fractions. These formulas are valid mainly for medium sized bodies ($100 < d < 1000$ m).

Chapter 6. The SolSyIn package

6.1 Package description

This package of programs (named after the "SOLar SYstem INtegrator") is extensively described in the reference [Berinde, 2001c]. We summarize here the main directions of its applicability

- obtaining the trajectory and orbital elements' variation for asteroids and comets;
- identification of close encounters with the Earth;
- long-term variation of MOID between two orbits;
- computing the LCE of a motion;

- identification of resonant motions;
- orbital uncertainty propagation of NEAs;
- obtaining impact conditions and the probability of impact with the Earth;
- evaluating the effect of radiative forces on small bodies' motion.

6.2 Radau-Everhart numerical integration method

An extensive mathematical description of this numerical algorithm [Everhart, 1984] and several improvements added to accurately handle the close encounters are described in the full paper. Estimates on its global integration error are also given.

The dynamical model in which the integrations are performed is also discussed. It ranges from classical newtonian perturbatrice forces (of the primary, respectively of the massive bodies)

$$\mathbf{F}_i^c = -G\frac{(M+m_i)}{r_i^3}\,\mathbf{r}_i, \tag{76}$$

$$\mathbf{F}_i^p = G\sum_{\substack{j=1\\ j\neq i}}^{n} m_j\left(\frac{\mathbf{r}_j-\mathbf{r}_i}{|\mathbf{r}_j-\mathbf{r}_i|^3}-\frac{\mathbf{r}_j}{r_j^3}\right), \tag{77}$$

to relativistic one

$$\mathbf{F}_i^c = \mathbf{F}_i^c + \frac{1}{c^2}\,\frac{GM}{r_i^3}\left[4\frac{GM}{r_i}\mathbf{r}_i - \left(\frac{\mathrm{d}\mathbf{r_i}}{\mathrm{d}t}\right)^2\mathbf{r}_i + 4\left(\frac{\mathrm{d}\mathbf{r_i}}{\mathrm{d}t}\cdot\mathbf{r_i}\right)\frac{\mathrm{d}\mathbf{r_i}}{\mathrm{d}t}\right]\,\mathbf{r}_i, \tag{78}$$

and radiative one

$$\mathbf{F}_i^c = \mathbf{F}_i^c + \frac{\beta_i G}{r_i^3}\,\mathbf{r_i} - \frac{1}{c}\,\frac{\beta_i G}{r_i^2}\left[\left(\frac{\mathrm{d}\mathbf{r_i}}{\mathrm{d}t}\cdot\mathbf{r_i}\right)\frac{\mathbf{r_i}}{r_i^2}+\frac{\mathrm{d}\mathbf{r_i}}{\mathrm{d}t}\right]. \tag{79}$$

6.3 A numerical example

At the end, a numerical example is formulated, for the asteroid 1999 AN_{10}, the first candidate for the closest encounter with our planet in this century, so far (figure 23).

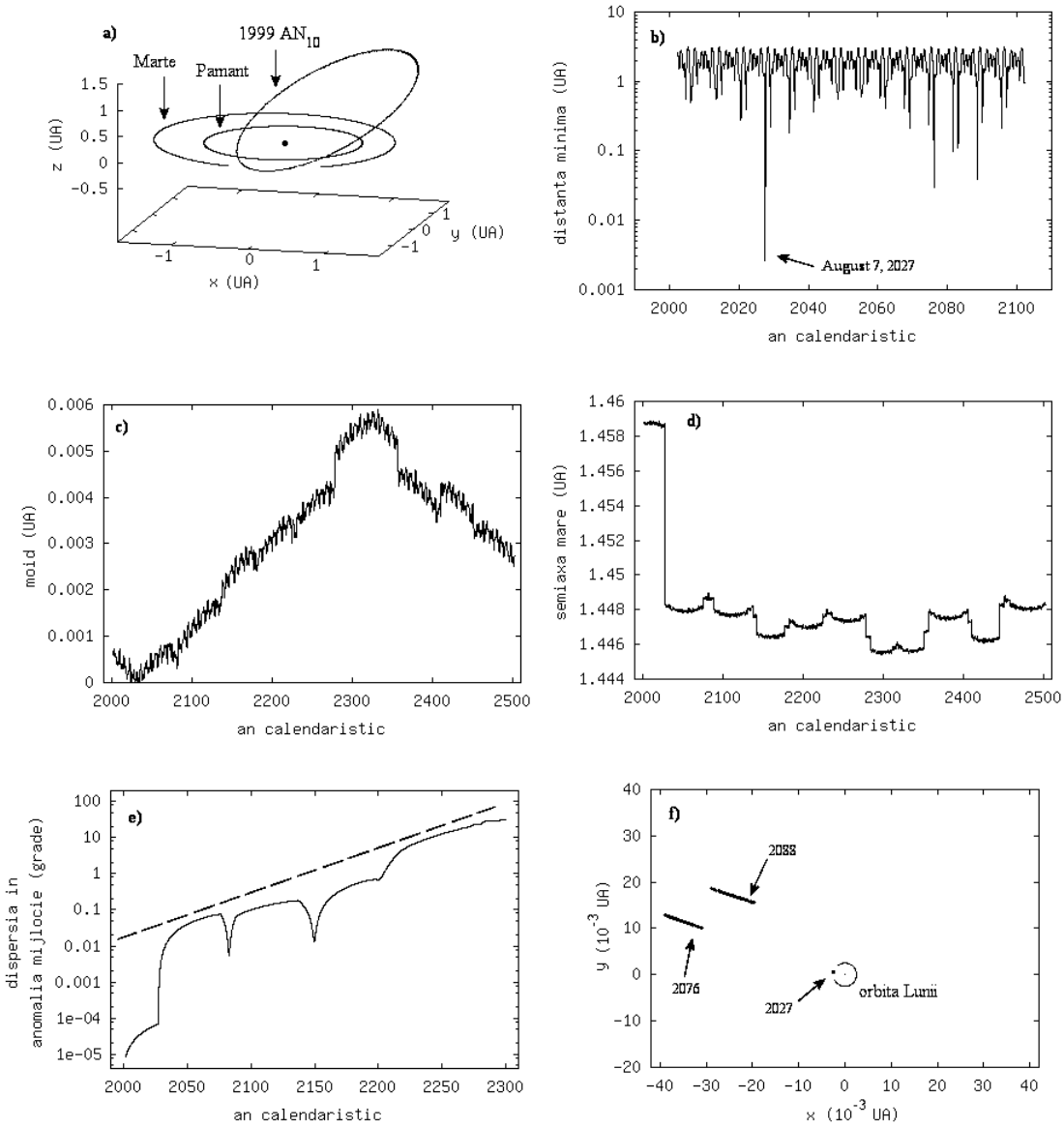

Figure 23: Some dynamical characteristics of the asteroid 1999 AN_{10}. a) its highly inclined orbit in space, b) distance variation to Earth (the minimum distance is 0.00261 UA), c) MOID variation (long-time orbital approach), d) semimajor axis variation (Geographos class), e) LCE computation (Lyapounov time $\approx$ 35 years) and f) the images of uncertainty region on the target plane, during three close encounters (corresponding years are given).

Selected references

[Berinde, 1999a] S. Berinde: 1999. *Some characteristics of the near-Earth asteroids population*, in Proceedings of the International Symposium on Astrophysics Research and Science Education, Castel Gandolfo 1998, edited by C. Impey, Vatican Observatory Foundation, p. 99.

[Berinde, 1999b] S. Berinde: 1999. *Statistical results on discovered near-Earth asteroids*, in Proceedings of the IAU Colloquium 173 "Evolution and Source Regions of Asteroids and Comets", Tatranska Lomnica 1998, edited by J. Svoren, E.M. Pittich and H. Rickman, Astronomical Institute of the Slovak Academy of Sciences, p. 81.

[Berinde, 2001a] S. Berinde: 2001. *Effects of multiple planetary encounters on Kuiper belt objects*, in Highlights of Astronomy vol. 12, Proceedings of Joint Discussion 4 "The Trans-Neptunian Population", The XXIV-th IAU General Assembly, Manchester 2000, edited by B. Bezard and J. Spencer, Astronomical Society of the Pacific, extended abstract.

[Berinde, 2001b] S. Berinde: 2001. *A quantitative approach of the orbital uncertainty propagation through close encounters*, in "Dynamics of Natural and Artificial Celestial Bodies", Proceedings of the US/European Celestial Mechanics Workshop, Poznań 2000, edited by H. Prętka-Ziomek, E. Wnuk, P.K. Seidelmann and D. Richardson, Kluwer Academic Publishers, p. 289.

[Berinde, 2001c] S. Berinde: 2001. *The SolSyIn package - An integrator for our solar system*, Internet Release (http://math.ubbcluj.ro/∼sberinde/solsyin).

[Berinde, 2002] S. Berinde: 2002. *An iterative Monte-Carlo method for finding virtual impactors among near-Earth asteroids*, "Asteroids, Comets, Meteors Conference 2002", Berlin, 29 July - 2 August 2002, paper submitted for communication.

[Binzel, 1997] R.P. Binzel: 1997. *A near-Earth object hazard index* in "Near Earth Objects. The United Nations International Conference", edited by J. Remo, New-York, p. 545.

[Bottke *et al.*, 2000] W.F. Bottke Jr, R. Jedicke, A. Morbidelli, J.M. Petit, B. Gladman: 2000. *Understanding the distribution of near-Earth asteroids*, Science, **288**, p. 2190.

[Bowell *et al.*, 1989] E. Bowell, B. Hapke, D. Domingue, K. Lumme, J. Peltoniemi, A.W. Harris: 1989. *Application of photometric models to asteroids*, in "Asteroids II", edited by P. Binzel, T. Gehrels, M.S. Matthews, The University of Arizona Press, p. 524.

[Carusi and Dotto, 1996] A. Carusi, E. Dotto: 1996. *Close Encounters of Minor Bodies with the Earth*, Icarus, **124**, p. 392.

[Carusi *et al.*, 1990] A. Carusi, G.B. Valsecchi, R. Greenberg: 1990. *Planetary close encounters: geometry of approach and post-encounter orbital parameters*, Celestial Mechanics and Dynamical Astronomy, **49**, p. 111.

[Chesley *et al.*, 2001] S.R. Chesley, A. Milani, G.B. Valsecchi, D.K. Yeomans: 2001. *Quantifying the risk posed by potential Earth impacts*, Asteroids 2001 Conference, Palermo, preprint.

[Dvorak, 1999] R. Dvorak: 1999. *The long term evolution of Atens and Apollos*, in Proceedings of the IAU Colloquium 173 "Evolution and Source Regions of Asteroids and Comets", Tatranska Lomnica 1998, edited by J. Svoren, E.M. Pittich and H. Rickman, Astronomical Institute of the Slovak Academy of Sciences, p. 59.

[Everhart, 1984] E. Everhart: 1984. *An efficient integrator that uses Gauss-Radau spacings*, in "Dynamics of Comets: Their Origin and Evolution", edited by A. Carusi and G.B. Valsecchi, D. Reidel, p. 185.

[Farinella *et al.*, 1994] P. Farinella, Ch. Froeschlé, R. Gonczi: 1994. *Meteorite delivery and transport*, in "Asteroids, Comets, Meteors 1993", Proceedings of the 160th Symposium of the International Astronomical Union, Italy, edited by A. Milani, M. di Martino and A. Cellino, Kluwer Academic Publishers, p. 189.

[Froeschlé and Morbidelli, 1994] Ch. Froeschlé, A. Morbidelli: 1994. *The secular resonances in the solar system*, in "Asteroids, Comets, Meteors 1993", Proceedings of the 160th Symposium of the International Astronomical Union, Italy, edited by A. Milani, M. di Martino and A. Cellino, Kluwer Academic Publishers, p. 189.

[Fujiwara *et al.*, 1989] A. Fujiwara, P. Cerroni, D.R. Davis, E. Ryan, M. di Martino, K. Holsapple, K. Housen: 1989. *Experiments and scaling laws on catastrophic collisions*, in "Asteroids II", edited by P. Binzel, T. Gehrels, M.S. Matthews, The University of Arizona Press, p. 240.

[Greenberg and Nolan, 1989] R. Greenberg, M.C. Nolan: 1989. *Delivery of asteroids and meteorites to the inner solar system*, in "Asteroids II", edited by P. Binzel, T. Gehrels, M.S. Matthews, The University of Arizona Press, p. 778.

[Greenberg and Nolan, 1993] R. Greenberg, M.C. Nolan: 1993. *Dynamical relationships of near-Earth asteroids to main-belt asteroids*, in "Resources of near-Earth space", edited by S. Lewis, The University of Arizona Press, p. 473.

[Hills and Goda, 1993] J.G. Hills, M.P. Goda: 1993. *The fragmentation of small asteroids in the atmosphere*, The Astronomical Journal, **105**, 3, p. 1114.

[Janiczek *et al.*, 1972] P.M. Janiczek, P.K. Seidelmann, R.L. Duncombe: 1972. *Resonances and encounters in the inner solar system*, The Astronomical Journal, **77-9**, p. 329.

[Milani and Mazzini, 1997] A. Milani, G. Mazzini: 1997. *Sistemi dinamici*, Proiect HyperText-Book, Internet (http://copernico.dm.unipi.it/∼milani/dinsis/dinsis.html).

[Milani, 1998] A. Milani: 1998. *Dynamics of planet-crossing asteroids*, Maratea NATO-ASI invited paper, edited by A.E. Roy and B. Steves.

[Milani, 1999] A. Milani: 1999. *The asteroid identification problem I: recovery of lost asteriods*, Icarus **137**, p. 269.

[Milani and Valsecchi, 1999] A. Milani, G.B. Valsecchi: 1999. *The asteroid identification problem II: target plane confidence boundaries*, Icarus **140**, p. 408.

[Milani *et al.*, 2000a] A. Milani, S.R. Chesley, A. Boattini, G.B. Valsecchi: 2000. *Virtual impactors: Search and destroy*, Icarus **145**, p. 12.

[Milani *et al.*, 2000b] A. Milani, S.R. Chesley, G.B. Valsecchi: 2000. *Asteroid close encounter with Earth: Risk assessment*, Planetary and Space Science **48**, p. 945.

[Murray and Dermott, 1999] C.D. Murray, S.F. Dermott: 1999. *Solar System Dynamics*, Cambridge University Press.

[Muller and Dvorak, 1995] P. Muller, R. Dvorak: 1995. *A survey of the dynamics of main belt asteroids. II*, Astronomy and Astrophysics, **300**, p. 289.

[Öpik, 1963] E. Öpik: 1963. *Survival of comet nuclei and the asteroids*, Advances in Astronomy and Astrophysics, **2**, p. 219.

[Press *et al.*, 1997] W.H. Press, S.A. Teukolsky, W.T. Vetterling, B.P. Flannery: 1997. *Numerical Recipes in Fortran 77. The Art of Scientific Computing*, Second edition, Cambridge University Press.

[Rabinowitz *et al.*, 1994] D. Rabinowitz, E. Bowell, E.M. Shoemaker, K. Muinonen: 1994. *The population of Earth-crossing asteroids*, in "Hazards due to Comets and Asteroids", edited by T. Gehrels, University of Arizona Press, Tucson, p. 285.

[Sekanina and Yeomans, 1984] Z. Sekanina, D.K. Yeomans: 1984. *Close encounters and collisions of comets with the Earth*, The Astronomical Journal, **89**, 1, p. 154.

[Steel and Baggaley, 1985] D.I. Steel, W.J. Baggaley: 1985. *C*ollisions in the solar system -I. Impacts of the Apollo-Amor-Aten asteroids upon the terrestrial planets, MNRAS, **212**, p. 817.

[Tisserand, 1896] F. Tisserand: 1896. *Traité de mécanique céleste*, Tome IV, Gauthier-Villars, Paris.